J Solid State Electrochem (2014) 18:3003–3010
DOI 10.1007/s10008-014-2493-0

ORIGINAL PAPER

PtIr–WO_3 nanostructured alloy for electrocatalytic oxidation of ethylene glycol and ethanol

Magdalena Murawska · James A. Cox · Krzysztof Miecznikowski

Received: 30 December 2013 / Revised: 25 April 2014 / Accepted: 27 April 2014 / Published online: 10 May 2014

Abstract In this article, we characterized tungsten oxide-decorated carbon-supported PtIr nanoparticles and tested it for the electrooxidation reactions of ethylene glycol and ethanol. Phase and morphological evaluation of the proposed electrocatalytic materials are investigated employing various characterization techniques including X-ray diffraction (XRD) and transmission electron microscopy (TEM). Electrochemical diagnostic measurements such as cyclic voltammetry, chronoamperometry, and linear sweep voltammetry revealed that the tungsten oxide-modified PtIr/Vulcan nanoparticles have higher catalytic activity for ethylene glycol and ethanol electrooxidation than that of PtIr/Vulcan. A significant enhancement for electrooxidation of CO-adsorbate monolayers occurred in the presence of a transition metal oxide relative to that of pure PtIr/Vulcan electrocatalyst. The likely reasons for this are modification on the Pt center electronic structure and/or increasing the population of reactive oxo groups at the PtIr/Vulcan electrocatalytic interface in different potential regions.

Keywords PtIr nanoparticles · Tungsten oxide · Ethylene glycol electrooxidation · Ethanol oxidation · Electrocatalysis

Introduction

An important task in the twenty-first century is to further develop fuel cells as alternative electrochemical devices for efficient generation of electricity. The low-temperature acid-type systems, such as hydrogen-oxygen polymer electrolyte membrane fuel cells and direct alcohol fuel cells, are, at present, the most commonly studied devices in many laboratories worldwide [1, 2]. Among organic compound fuels for anodic reactions in fuel cells, methanol has been historically most extensively studied [3], and more recently, other short chain liquid fuels such as ethanol and ethylene glycol have become important [4–11]. In the case of direct methanol fuel cells (DMFC), slow electrode kinetics of methanol oxidation and methanol adsorption products (which is mainly CO_{ads}) poisoning the surface of Pt electrode at low temperature still hamper application [3, 12–15]. As a result, new fuels and new catalysts remain important research topics.

Polyhydric and monohydric (except methanol) alcohols, such as ethylene glycol and ethanol, have been proposed as potential FC fuels which are much less volatile and less toxic than methanol. Moreover, both alcohols have some of the largest volumetric energy densities, and they involve the transfer of a number of electrons that set a practical challenge for the effectiveness of catalysts. They also show lower permeability through membranes (lower crossover effect) [16–18]. However, the electrochemical oxidation of short chain alcohol (monohydric or polyhydric alcohols) is much more complex than, for example, H_2 oxidation. The main challenge generally for electrooxidation of polyhydric and monohydric alcohols to carbon dioxide is associated with the cleavage of the C–C bond for complete conversion. Due to incomplete oxidation, various intermediate species from electrooxidation in both alcohols are observed.

It is well established that Pt is rated as the most active material for oxidation of small organic molecules in acidic media, but poisoning by the intermediate by-product of CO-adsorbed species of the binary or ternary platinum-based alloys with Ru, Sn, Rh, Pb, W, or Mo [19–27] was proposed to enhance the electrooxidation activity toward alcohols.

M. Murawska · K. Miecznikowski (✉)
Department of Chemistry, University of Warsaw, Pasteura 1, PL-02-093 Warsaw, Poland
e-mail: kmiecz@chem.uw.edu.pl

J. A. Cox
Department of Chemistry and Biochemistry, Miami University, Oxford, OH 45056, USA

Alternatively, Ir has also been employed as a co-metal for platinum-based catalysts in unitized polymer electrolyte fuel cells because of its high stability and resistance to corrosion [28, 29]. The presence of Ir, particularly IrO_2, enhances the electrooxidation of methanol in direct methanol fuel cells due to providing a large number of OH groups that are adsorbed at relatively low potentials [30–34]. Moreover, Cao et al. reported that the addition of Ir into Sn showed to be a promising alternative for Pt-based catalysts for ethanol electrooxidation [35]. Tremiliosi-Filho et al. demonstrated a positive effect for ethanol oxidation in which IrO_2 was incorporated to platinum-based catalysts [36]. Recently, Adzic et al. revealed that the presence of a high content of Ir atoms into ternary catalyst $PtIr/SnO_2/C$ enhances the complete electrooxidation of ethanol to CO_2 at a relatively low-onset potential [34]. Furthermore, PtIr catalysts have been utilized for electrooxidation of ethylene glycol with positive results [37, 38].

One of the numerous approaches to increase the electrocatalytic activity of platinum-based catalysts toward the oxidation of small organic compounds is the use of transition metal oxides as support systems for catalytic metal sites. The presence of transition metal oxides in the neighborhood of catalytic sites of noble metal catalysts results in an increasing population of –OH groups at low potentials, thereby mitigating CO poisoning of catalytically active platinum centers, possibly facilitating the cleavage of C–H bonds as well as in a weakening of C–C bonds. This assumption is in accord with reports in which a significant improvement in oxidation of small organic molecules with metal oxides (e.g., WO_3, MoO_3, TiO_2, ZrO_2, V_2O_5, and CeO_2) modified by Pt-based alloy catalysts has been observed [8, 9, 39–43].

The present work will concentrate on the preliminary investigation of a carbon-supported PtIr-based anodic catalyst with tungsten oxide as the additive prepared by the adsorption of tungsten acid. Not only the peak current value during cyclic voltammetry (CV) tests in a broad potential region, but also the more specific performance in the low potential region will be evaluated from a more comprehensive point of view. Thus, the electrocatalytic activity toward ethanol and ethylene glycol oxidation in comparison with that of PtIr/C and WO_3-modified PtIr/C catalysts will be evaluated by CV, linear sweep voltammetry (LSV), and chronoamperometry (CA) methods.

Experimental

All chemicals were commercial materials of analytical grade purity that were obtained from Premetek PtIr/C nanoparticles (20 % on Vulcan XC-72, Pt:Ir 1:1). Solutions were prepared using doubly distilled and subsequently deionized (Millipore Milli-Q) water. Argon was used to de-aerate the solutions and to keep an oxygen-free atmosphere over the solution during the measurements. Some characteristics of catalytic particles were obtained using a LIBRA 120 transmission electron microscope (TEM) operating at 120 kV. Samples for TEM measurements were prepared by depositing drops of colloidal solutions of nanoparticles onto 400-mesh copper grids supporting a Fromvar film (Agar Scientific) and, later, drying them in ambient laboratory conditions (temperature, 20±2 °C) for 24 h prior to TEM analysis. X-ray diffraction (XRD) patterns of the catalysts were obtained with a Bruker D8 Discover operating with a Cu X-ray tube (1,5406 Å) and Vantec (linear) detector (k=1.5406 Å).

Electrochemical characterization was performed in a three-electrode, single compartment cell. The working electrode was glassy carbon, and the counter electrode was carbon rod. As a rule, all potentials in the present work were measured versus a K_2SO_4-saturated Hg_2SO_4 reference electrode and were recalculated and reported versus the reversible hydrogen electrode (RHE). CH Instruments 750 A workstations were used for all electrochemical measurements.

The catalyst layer was fabricated through modification of the working electrode by immobilization of PtIr/C nanoparticles. WO_3 modification of the PtIr/C catalyst was in accordance with the procedure described in our previous papers [8, 9]. Briefly, a solution of tungstic acid was prepared by passing an aqueous solution of 0.05 mol dm^{-3} Na_2WO_4 through a proton exchange resin. In a typical procedure, selected amount of PtIr/C catalyst was added to 2 cm^3 of 0.05 mol dm^{-3} aqueous solution of tungstic acid. The resulting suspension was stirred for 24 h. During that process, the PtIr/C nanoparticles interacted with tungstic acid to form tungsten oxide or hydrogen tungsten oxide bronzes. The supernatant solution was centrifuged and replaced with water in order to obtain a colloidal solution of tungsten oxide-modified PtIr/C nanoparticles that was stable for months. The Pt-to-tungsten ratio in the given catalyst system was determined with X-ray fluorescence (XRF); the targeted ratio was approximately 1:1.

To prepare a homogeneous catalyst layer on the glassy carbon working electrode surface, a 5-μl aliquot of the catalyst dispersion was deposited using a micropipette (the nominal loading of catalyst was approximately 160 μg cm^{-2}) and allowed to dry under ambient conditions. Prior to this step, the suspensions were treated in an ultrasonic bath for 5 min. When the catalyst layers had dried, 2 μl of Nafion (0.02 % alcoholic solution) was dropped on top of the glassy carbon electrode surface covered with the catalyst and dried at room temperature. Prior to the electrooxidation processes, the catalytic electrodes were scanned with 25 complete oxidation/reduction cycles between 0.0 and 0.8 V in 0.5 mol dm^{-3} H_2SO_4 at 50 mV s^{-1} scan rate.

The CO-stripping experiments were carried out in 0.5 mol dm^{-3} H_2SO_4 electrolyte utilizing the glassy carbon electrode substrate onto which surface the appropriate catalyst

was introduced. As a rule, a few cyclic voltammetric measurements (at 50 mV s^{-1}) were recorded in the potential range from 0.0 to 0.8 V in the deoxygenated electrolyte. The CO-saturated solution was prepared by flowing pure CO (from Air Liquide) through the electrolyte for 10 min. The CO adsorption process that was employed (mainly on the surface of catalytic Pt nanocenters) was achieved by underpotential control at 0.1 V versus RHE for 5 min, after which the dissolved CO was removed from the electrolyte by bubbling argon for 30 min maintaining the applied potential (0.1 V), in order to have a solution free of CO. Then, the adsorbed CO monolayer was stripped by recording three cyclic voltammetric scans in the potential range from 0.0 to 0.9 V at a scan rate of 10 mV s^{-1}. The measurements using these catalysts were repeated three or four times with freshly prepared electrodes, and the average results are presented here.

Results and discussion

The X-ray patterns of the PtIr/Vulcan nanoparticles in the presence and absence of the WO_3 modifier are shown in Fig. 1a, b. The broad diffraction peak centered at 20.0–25.0° in all the XRD pattern is attributed to the hexagonal carbon support [44]. In the case of unmodified PtIr/Vulcan nanoparticles, the other characteristic peaks at ca. 39.5°, 46.3°, and 67.7° correspond to the Pt lattice planes (PCPDF 04-0802) [45, 46]. The diffractogram of the WO_3-modified PtIr/Vulcan electrocatalyst shows peaks at 2θ=40.5°, 46.9°, and 66.2°, which are associated with Pt reflections and the signals that originated from WO_3 (PCPDF 43-0679). The results indicate that Pt fcc is the main crystalline phase in the catalysts and that the presence of tungsten species resulted in the formation of crystalline aggregates. A peak shift is observed which could indicate the interaction between PtIr/Vulcan alloy and tungsten oxide. Of the XRD patterns, none were metallic Ir, or iridium oxide diffraction peaks have been observed because Pt and Ir metals have similar diffraction peak positions and crystalline structures [33, 36]. To estimate the average particle sizes from Scherrer's equation, the Pt peak (at 2θ=39.5°) was used [46]. The latter peak was chosen because it is located in a region where there are no interferences from the carbon support. The average Pt particle sizes were obtained from the position and the full-width at half-maximum values of the Pt peak (at 2θ=39.5°). The values were in the ranges from 4 to 6 and 6 to 8 nm for unmodified and modified PtIr/Vulcan nanoparticles, respectively. Higher values of the average particle sizes for the WO_3-modified PtIr/Vulcan can be interpreted in terms of deposition of the WO_3 crystalline monoclinic structure.

In order to get more information about the size, morphology, and distribution of nanoparticles on the carbon material, TEM analysis was performed. Figure 2 shows the TEM images and distributions of the series of PtIr/C and WO_3-modified PtIr/C nanoparticles. Low magnification images show that the supported material was predominantly irregular spheres or spheroids of bimetallic nanoparticles that were homogeneously dispersed on the carbon (Vulcan XC-72) surfaces. The average particle sizes lie in the narrow range of 5–8 nm with a standard deviation of 1 nm, which is in agreement with the XRD results for WO_3-modified PtIr/Vulcan and unmodified PtIr/Vulcan catalysts.

For initial electrochemical characterization, cyclic voltammetric curves of the PtIr/Vulcan and the WO_3-modified PtIr/Vulcan nanoparticles deposited on glassy carbon electrode were obtained in 0.5 mol dm^{-3} sulfuric acid-supporting electrolyte (Fig. 3). In both cases, slight changes in the shape or current values of the cyclic voltammetric curves are observed. In the hydrogen adsorption/desorption region (between 0.0 and 0.4 V versus RHE) for the all proposed catalysts, some changes in the voltammetry are seen because of the dependence on the surface composition. The voltammogram for unmodified PtIr/Vulcan (Fig. 3a) is characterized by a single large peak in the hydrogen adsorption/desorption region, whereas the electrochemical behavior of

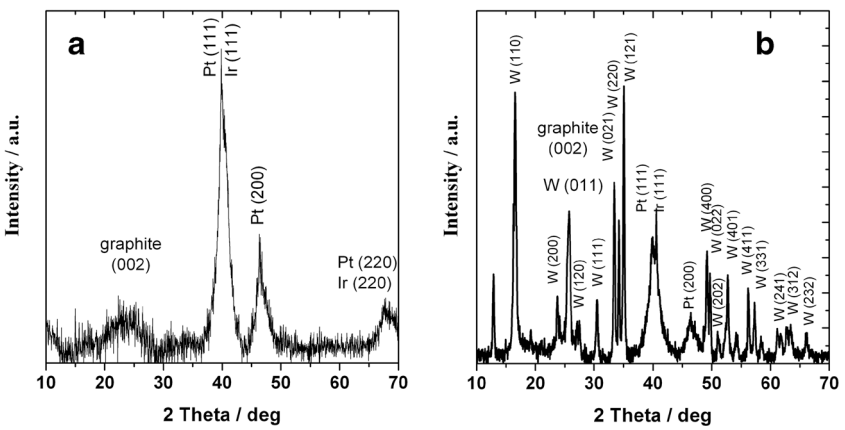

Fig. 1 XRD diffractograms of PtIr/Vulcan (**a**) and WO_3-modified PtIr/Vulcan (**b**)

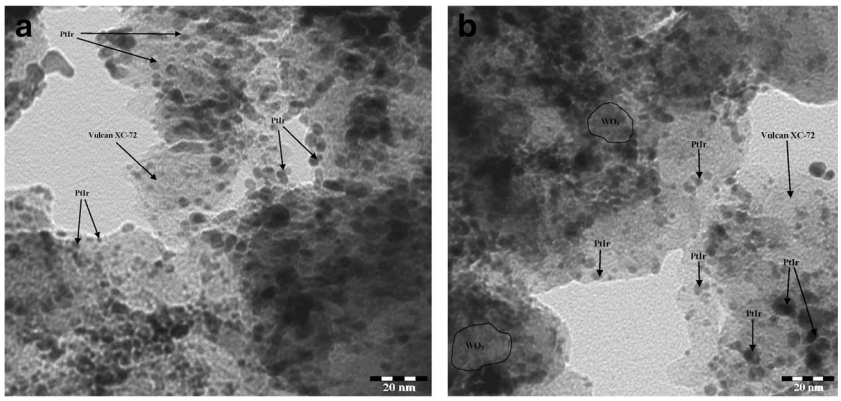

Fig. 2 Low magnification micrographs (TEM) of PtIr/Vulcan (**a**) and WO_3-modified PtIr/Vulcan (**b**)

electrodes made from the WO_3-modified PtIr/Vulcan nanoparticles (Fig. 3b) shows two peaks in this region. Moreover, in the double layer region, which is between 0.4 and 0.7 V versus RHE, significant currents are recorded. This behavior is typical of electrocatalysts composed of transition metals dispersed on a carbon black support [36]. It is apparent from Fig. 3b that the oxidation peak appearing at about 0.2 V most likely reflects the intercalation of protons in tungsten oxide (WO_3) and tends to overlap with the hydrogen adsorption/desorption region of bare platinum (at a potential lower than 0.4 V). This interpretation is difficult to prove because of the problem of unambiguously distinguishing contributions from the reversible reduction of tungsten oxide to hydrogen tungsten bronzes from the abovementioned hydrogen adsorption and desorption peaks originating from Pt and Ir.

The behavior of the proposed catalytic layers was tested toward ethanol and ethylene glycol electrooxidation processes. Representative cyclic voltammograms of these species at both PtIr/Vulcan and WO_3-modified PtIr/Vulcan electrocatalysts deposited on glassy carbon electrode are shown in Fig. 4. The cyclic voltammograms of ethanol (Fig. 4a) and ethylene glycol (Fig. 4b) obtained at the PtIr/Vulcan and WO_3-modified PtIr/Vulcan surface, respectively, show well-defined peaks for both forward and reverse scans in the investigated potential region. In the forward scan, the ethanol oxidation current at PtIr/Vulcan catalysts starts (at 0.3 V) and reaches the peak at 0.87 V, which is located at the same potential as compared to the WO_3-modified PtIr/Vulcan, as illustrated in Fig. 4a. In the reverse scan, a single peak is developed at 0.7 V, which can be attributed to the oxidative decomposition of by-products [16].

Similar measurements to those presented in Fig. 4b were performed with ethylene glycol. The cyclic voltammograms of WO_3-modified PtIr/Vulcan and bare PtIr/Vulcan in the presence of ethylene glycol exhibited no significant oxidation current up to 0.27 and 0.35 V, respectively. Two distinct peaks were observed in the potential range between 0.4 and 0.9 V in comparison to previous literature reports [36–38], and these processes can be attributed primarily to the oxidation of adsorbed organic species. In the case of electrooxidation of ethylene glycol, various intermediate oxidation products can be expected according to spectroscopic data [47–52] including CO, glycol aldehyde, glycolate, glyoxylate, oxalate, and formate. This is in contrast to the data obtained with ethanol, the oxidation of which produces only CH_2COOH, CO_2, and CH_3CHO [53].

Generally, in the presence of both fuels, the current density in the hydrogen region decreases in comparison to the voltammograms obtained in the supporting electrolyte alone due to their adsorption. Additionally, Fig. 4 displays that in both cases, the current density values are higher in the tested potential range confirming the enhancement of the electrooxidation of ethanol and ethylene glycol by the presence of the metal oxide WO_3. In addition, the onset potentials of ethanol and ethylene glycol oxidation shift toward more

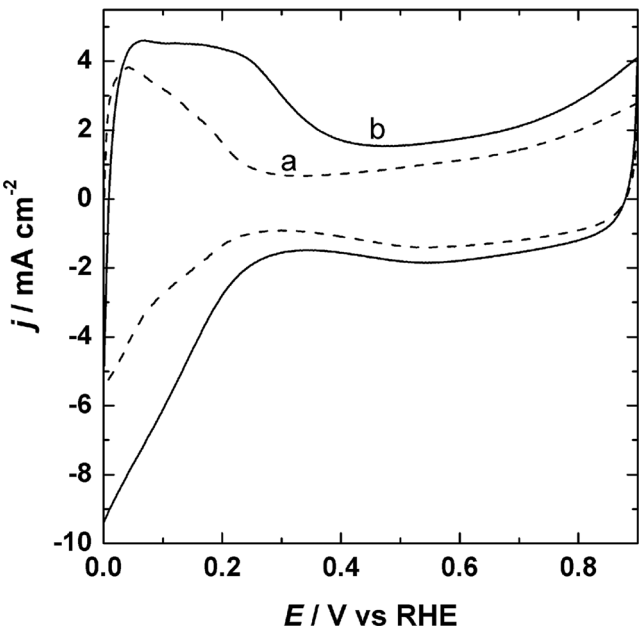

Fig. 3 Cyclic voltammetric responses of PtIr/Vulcan (*a*) and WO_3-modified PtIr/Vulcan (*b*) catalytic systems in 0.5 mol dm^{-3} H_2SO_4. Scan rate= 10 mV s^{-1}

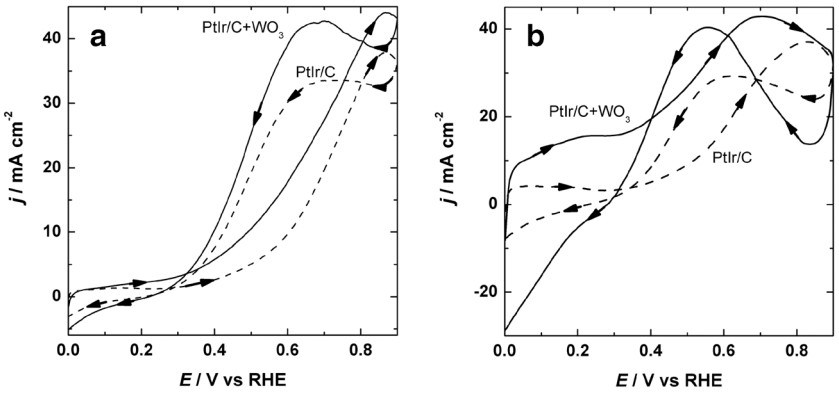

Fig. 4 Cyclic voltammetric responses for oxidation of 0.5 mol dm^{-3} ethanol (**a**) with PtIr/Vulcan (*a*) and WO_3-modified PtIr/Vulcan (*b*) and 0.5 mol dm^{-3} ethylene glycol (**b**) with PtIr/Vulcan (*a*) and WO_3-modified PtIr/Vulcan (*b*) catalysts. Electrolyte = 0.5 mol dm^{-3} H_2SO_4. Scan rate = 10 mV s^{-1}

negative values which is especially pronounced in the case of ethylene glycol oxidation. This can be explained by the fact that transition metal oxides (e.g., WO_3 and related compounds) are known to activate interfacial water molecules (from –OH groups on WO_3) at lower potentials which, in turn, promote the removal of poisoning species from the noble metal catalyst [8, 9, 14, 54–60].

Figure 5 exhibits background-subtracted linear scan voltammograms (LSVs) for ethanol and ethylene glycol electrooxidation on PtIr/Vulcan and WO_3-modified PtIr/Vulcan electrocatalysts deposited on glassy carbon substrate recorded in the potential range of 0.0–0.9 V. As can be seen for both fuels, the shape of the LSV curves is almost the same in the examined potential range. The only difference is that the current densities are higher for WO_3-modified PtIr/Vulcan nanoparticles than those recorded on bare PtIr/Vulcan nanoparticles. This behavior is obvious in the case of ethylene glycol oxidation. The LSV experiments also confirm the shifting of the onset potential for ethanol and ethylene glycol electrooxidation on WO_3-modified PtIr/Vulcan catalysts toward lower potential values. It is likely that the increases of the oxidation current densities observed in the LSV curves are associated with the addition of tungsten oxide. The decrease of the onset potential of ethylene glycol and ethanol oxidation is due to activation of interfacial water molecules forming –OH species at lower anodic potential than the bare catalyst.

The effect of temperature for ethanol and ethylene glycol electrooxidation in bare and WO_3-modified PtIr/Vulcan nanoparticles was also investigated. When the temperatures increase from 10 to 50 °C, the oxidation current densities for both become higher. Based on the Arrhenius equation, the activation energy (45 and 49 kJ mol^{-1}, respectively) can be determined from the slope calculated by linear regression by plotting ln(*j*) as a function of reciprocal of temperature (figure not shown). The value of activation energy is in good agreement with a previous report on alcohol electrooxidation [61]. This observation suggests that the increase of temperature causes more facile oxidation kinetics and decreases poisoning by the intermediate species.

In order to evaluate the electrocatalytic activity and also the long-term stability of tungsten oxide-modified PtIr/Vulcan nanoparticles for ethanol and ethylene glycol oxidation, chronoamperometric measurements were performed at low potentials (Fig. 6). The polarization current density for the electrooxidation of both fuels on the investigated catalytic systems displays a rapid decrease in the first period of the experiment before reaching a stable value. The catalytic current developed for tungsten oxide-modified PtIr/Vulcan electrocatalysts for both ethanol and ethylene glycol always

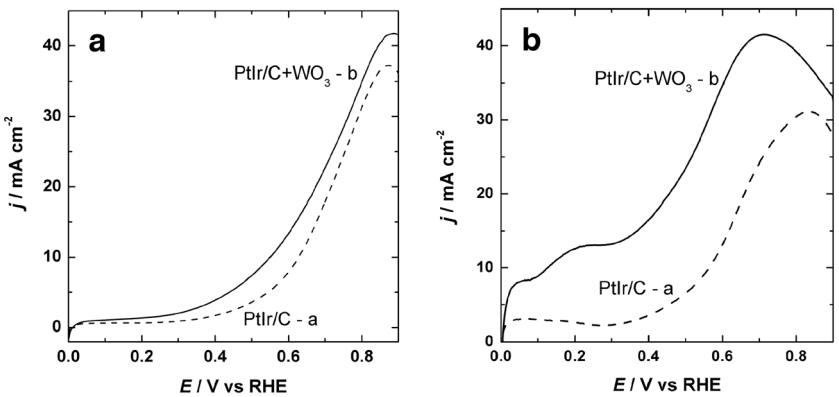

Fig. 5 Linear scan voltammetry responses for oxidation of 0.5 mol dm^{-3} ethanol (**a**) with PtIr/Vulcan (*a*) and WO_3-modified PtIr/Vulcan (*b*) and 0.5 mol dm^{-3} ethylene glycol (**b**) with PtIr/Vulcan (*a*) and WO_3-modified PtIr/Vulcan (*b*) catalyst at 10 mV s^{-1} scan rate. Electrolyte=0.5 mol dm^{-3} H_2SO_4

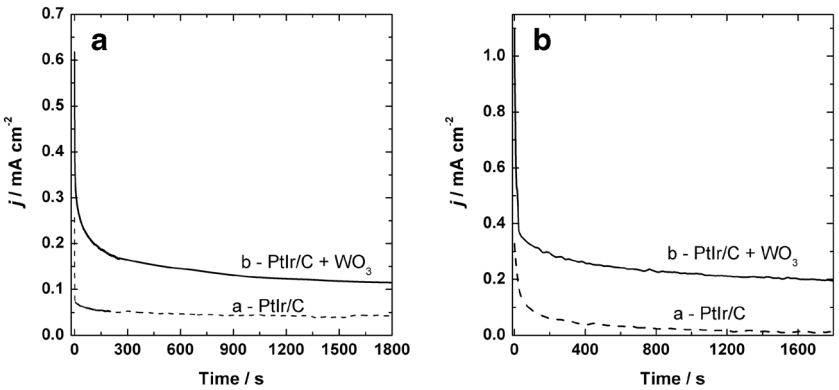

Fig. 6 Chronoamperometric current-time responses (recorded at 0.3 V) for oxidation of 0.5 mol dm^{-3} ethanol (**a**) with bare PtIr/Vulcan (*a*) and WO_3-modified PtIr/Vulcan (*b*) and 0.5 mol dm^{-3} ethylene glycol (**b**) with PtIr/Vulcan (*a*) and WO_3-modified PtIr/Vulcan (*b*) catalysts. Electrolyte= 0.5 mol dm^{-3} H_2SO_4

was significantly higher than those produced for bare PtIr/Vulcan nanoparticles in the tested time period. These results are consistent with those obtained by cyclic voltammetry. In the initial phase of the chronoamperometric experiments, it is likely that a higher number of free active sites are available for adsorbed ethanol or ethylene glycol molecules (fast kinetic rate reaction), and during the next few minutes (rate determining step), the amount of free catalyst sites is limited by poisoning by intermediate species, such as CO, CH_x, CH_3CHO, CH_3COOH (for ethanol oxidation), glycol aldehyde, glycolate, glyoxylate, oxalate, and glycolate (for ethylene glycol). In this regard, the improvement of catalytic properties observed by introduction of WO_3 on Pt-based nanoparticles surface can be associated with the oxophilic nature of tungsten oxide providing hydroxyl groups (–OH) on the oxide surface at lower potential, which promotes electrooxidation of the surface CO-poisoning intermediates species [8, 9, 54–60].

Regarding the stability of the electrocatalytic responses in the presence of ethylene glycol and ethanol, the long-term chronoamperometric and repetitive voltammetric measurements of WO_3-modified PtIr/C and bare PtIr/C systems have been performed (not shown here) under the same conditions. In the potential range between 0.0 and 0.9 V, the catalytic peak currents decreased, remaining at 90 % than those of the first cycle after 100 cycles when the WO_3-modified system has been used. During long-term chronoamperometric experiments (1 h), there was only 15 % decrease of catalytic currents in the case of tungsten oxides. In both experiments, no significant deactivation effect was observed that may imply dissolution of WO_3.

In order to gather information of the ability of CO_{ads} poisoning species to undergo oxidative desorption from the surface of the prepared Pt-based catalysts, CO-stripping voltammetry was performed. A typical CO_{ads}-stripping curve on bare PtIr/Vulcan catalyst is presented in Fig. 7a. It is characterized by a single sharp and prominent CO_{ads} oxidation peak centered at 0.69 V with a CO_{ads} oxidation onset potential of 0.590 V. In contrast, for the WO_3-modified PtIr/Vulcan catalysts, two separated CO_{ads} oxidation peaks with the position of the main peak potential at 0.62 V were found in the stripping voltammetric method (Fig. 7b). The onset potential for the main CO_{ads} oxidation peak starts near 0.49 V. It becomes broadened and shifts to a more negative potential (ca. 100 mV) versus the main CO_{ads} oxidation peak for the bare PtIr/Vulcan. For both catalysts, the hydrogen region was completely blocked by the full coverage with CO_{ads}; the main CO-stripping (oxidation) peak appeared only during the first anodic cyclic, which indicates that all adsorbed CO was oxidized and removed from the surface under this condition. This observation is in good agreement with the previous reports for metal oxides (e.g., WO_3, MoO_3) [8, 9, 62, 63].

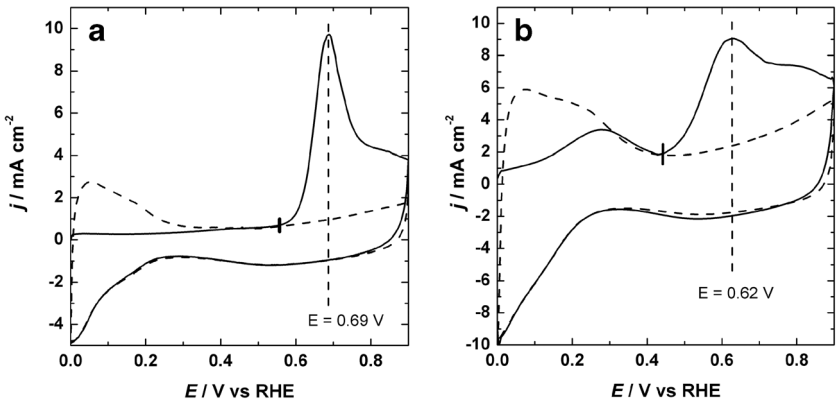

Fig. 7 CO-stripping voltammograms recorded at 10 mV s^{-1} in 0.5 mol dm^{-3} H_2SO_4 for the PtIr/Vulcan (**a**) and WO_3-modified PtIr/Vulcan (**b**) catalysts. CO adsorption was done at 0.1 V. *Solid curve* shows the first cycles, while the *dot curve* shows the second cycles

The presence of two peaks on the CO-stripping voltammetry has been described in the literature [64–68]. Two signals observed for oxidation of CO-adsorbed curve on the WO_3-modified PtIr/Vulcan catalyst suggest that two active sites for CO_{ads} oxidation may exist, which are the likely case due to a variation in the interaction with the metal oxide. In a previous report, this effect for Pt-based electrode has been explained by the presence of at least two different types of CO adsorption products (linearly or bridged bound) which are characterized by different binding energies [69]. Moreover, the peak that appears at the lower potential may be ascribed the CO_{ads} oxidation on the surface of WO_3-modified PtIr/Vulcan catalyst corresponding to the interaction between the Pt nanoparticles and tungsten oxide, whereas the peak at the higher potential may be attributed to adsorption on Pt nanoparticles at a large distance from tungsten oxide. Additionally, it cannot be excluded that this peak originates from the redox reaction of a tungsten species.

To estimate the electrochemically active surface area (S_A), the CO-stripping voltammetry method was used. The hydrogen adsorption/desorption system cannot be used because of the overlap with the redox process of tungsten oxide. The CO-stripping voltammetry method relies on forming a monolayer of strongly adsorbed CO on the bare and modified PtIr/Vulcan catalysts. Generally, CO may form a linear, bridge bond to the surface leading to different numbers of electrons per site (2 and 1, respectively). Those two CO adsorption configurations are strongly influenced by the applied potential. A linear adsorption may dominate if the CO adsorption occurs at a potential close to 0 V. By analogy to these conditions, it was assumed that one monolayer of CO adsorbed on Pt (linked linearly) and that the coulombic charge required to oxidize adsorbed CO to CO_2 is equal to 420 μC cm^{-2} [63, 70]. The charge value required to estimate the electrochemically active surface area was determined by integrating the main CO-stripping peaks. The obtained S_A values for the catalysts were 57 and 54 m^2 g^{-1} for bare PtIr/Vulcan and WO_3-modified PtIr/Vulcan, respectively. It is reasonable to conclude that the electrochemical active surface area is not the major factor causing the difference of their catalytic activities for ethylene glycol and for ethanol electrooxidations. In other words, tungsten oxide species occupied slightly the electrochemically active surface area of modified PtIr/Vulcan nanoparticles. The same tendency has been noticed by others with different catalysts (e.g., Pt, PtSn, and PtRh) and with various transition metal oxides [57, 62, 63, 71]. These effects may be explained by the ability of tungsten oxide in contact with aqueous solutions to increase the population of surface hydroxyl groups which likely play a major role in the CO_{ads} removal [55]. Further work is needed to determine whether such catalysts are stable under test conditions for fuel cells to elucidate full reaction pathways.

Conclusions

Herein, we demonstrate the enhancement of the activity of catalysts composed of bimetallic PtIr nanoparticles and tungsten oxide toward electrooxidation of ethylene glycol and ethanol. From both XRD and TEM results, the average particle sizes were found to be in the range of 4–8 nm and uniformly dispersed on glassy carbon. The adsorbed layer of tungsten oxide on PtIr/Vulcan nanoparticles increases the catalytic currents and decreases the onset potentials for electrooxidation of ethylene glycol and ethanol. The above electrochemical measurements confirmed that the presence of tungsten oxide on the surface is beneficial in the electrooxidation of ethylene glycol and ethanol. The results also showed that the activity of the PtIr/Vulcan nanoparticles for oxidation of poisoning species (CO_{ads}) is higher in the presence of tungsten oxide. The activation effect may involve direct specific interactions (chemical or electronic) between WO_3 and both Pt and Ir metals.

Acknowledgments The authors acknowledge the financial support from the National Science Centre (Poland), project No. 2011/03/B/ST4/02413. J.A.C. acknowledges the partial support of this work by the U.S. National Institutes of Health through grant R15GM087662-01.

References

1. Antolini E (2009) Appl Catal B Environ 88:1–24
2. Zhang J (2008) PEM fuel cell electrocatalysts and catalyst layers fundamentals and applications. Springer, Berlin
3. Liu H, Zhang J (2009) Electrocatalysis of direct methanol fuel cells. Wiley-Vch
4. Demarconnay L, Brimaud S, Coutanceau C, Leger JM (2007) J Electroanal Chem 601:169–180
5. Serov A, Kwak C (2010) Appl Catal B Environ 97:1–12
6. Halseid MC, Jusys Z, Behm RJ (2010) J Electroanal Chem 644:103–109
7. Feng YY, Yin WP, Li Z, Huang CD, Wang YX (2010) Electrochim Acta 55:6991–6999
8. Miecznikowski K, Kulesza PJ (2011) J Power Sources 196:2595–2601
9. Miecznikowski K (2012) J Solid State Electrochem 16:2723–2731
10. Kowal A, Li M, Shao M, Sasaki K, Vukmirovic MB, Zhang J, Marinkovic NS, Liu P, Frenkel AI, Adzie RR (2009) Nature Mater 8:325–330
11. Li ZY, Liang YJ, Jiang SP, Shan XD, Lin ML, Xu CW (2012) Fuel Cells 12:677–682
12. Kulesza PJ, Grzybowska B, Malik MA, Chojak M, Miecznikowski K (2001) J Electroanal Chem 512:110–118
13. Vijayaraghavan G, Gao L, Korzeniewski C (2003) Langmuir 19: 2333–2337
14. Barczuk PJ, Tsuchiya H, Macak JM, Schmuki P, Szymanska D, Makowski O, Miecznikowski K, Kulesza PJ (2006) Electrochem Solid-State Lett 9:E13–E16

15. Cheng Y, Jiang SP (2013) Electrochim Acta 99:124–132
16. Livshits V, Peled E (2006) J Power Sources 161:1187–1191
17. Liu H, Qiqan W, Wilkinson DP, Shen J, Wang H, Zhang J (2006) J Power Sources 154:202–213
18. Jablonski A, Lewera A (2012) Appl Catal B-Environ 115:25–30
19. Lamy C, Lima A, LeRhun V, Delime F, Countanceau C, Leger JM (2002) J Power Sources 105:283–296
20. Jusys Z, Schmidt TJ, Dubau L, Lasch K, Jorissen L, Garche L, Behm RJ (2002) J Power Sources 105:297–304
21. Neto AO, Giz MJ, Perez J, Ticianelli EA, Gonzalez ER (2002) J Electrochem Soc 149:A272–A279
22. Mann J, Yao N, Bocarsly AB (2006) Langmuir 22:10432–10436
23. Wang H, Jusys Z, Behm RJ (2006) J Power Sources 154:351–359
24. Colmati F, Antolini E, Gonzalez ER (2006) J Power Sources 157:98–103
25. Sen Gupta S, Datta J (2006) J Electroanal Chem 594:65–72
26. Li GC, Pickup PG (2006) Electrochim Acta 52:1033–1037
27. Neto AO, Dias RR, Tusi MM, Linardi M, Spinace EV (2007) J Power Sources 166:87–91
28. Ioroi T, Yasuda K (2005) J Electrochem Soc 152:A1917–A1924
29. Fatih K, Neburchilov V, Alzate V, Neagu R, Wang H (2010) J Power Sources 195:7168–7175
30. Reetz MT, Lopez M, Grunert W, Vogel W, Mahlendorf F (2003) J Phys Chem B 107:7414–7419
31. Tsaprailis H, Birss VI (2004) Electrochem Solid State Lett 7:A348–A352
32. Chen A, La Russa DJ, Miller B (2004) Langmuir 20:9695–9702
33. Liao S, Holmes KA, Tsaprailis H, Birss VI (2006) J Am Chem Soc 128:3504–3505
34. Li M, Cullen DA, Sasaki K, Marinkovic NS, More K, Adzic RR (2013) J Am Chem Soc 135:132–141
35. Cao L, Sun G, Li H, Xin Q (2007) Electrochem Commun 9:2541–2546
36. Ribeiro J, dos Anjos DM, Kokoh KB, Coutanceau C, Leger JM, Olivi P, de Andrade AR, Tremiliosi-Filho G (2007) Electrochim Acta 52:6997–7006
37. Neto AO, Vasconcelos TRR, Da Silva RWRV, Linardi M, Spinac EV (2005) J Appl Electrochem 35:193–198
38. Raghuram C, Keith S (2007) J Appl Electrochem 37:1077–1084
39. Maiyalagan T, Khan FN (2009) Catal Commun 10:433–436
40. Song H, Qiu X, Li F (2009) Appl Catal A-General 364:1–7
41. Anjos DMD, Kokoh KB, Leger JM, Andrade ARD, Olivi P, Tremiliosi-Filho G (2006) J Appl Electrochem 36:1391–1397
42. Ou DR, Mori T, Togasaki H, Takahashi M, Ye F, Drennan J (2011) Langmuir 27:3859–3866
43. Hepel M, Kumarihamy I, Zhong CJ (2006) Electrochem Commun 8:1439–1444
44. Wang J, Yin G, Shao Y, Zhang S, Wang Z, Gao Y (2007) J Power Sources 171:331–339
45. Zhou W, Zhou Z, Song S, Li W, Sun G, Tsiakaras P, Xin Q (2003) Appl Catal B Environ 46:273–285
46. Radmilovic V, Gasteiger HA, Ross PN Jr (1995) J Catal 154:98–106
47. Hahn F, Beden B, Kadirgan F, Lamy C (1987) J Electroanal Chem 216:169–180
48. Christensen PA, Hammet A (1989) J Electroanal Chem 260:347–359
49. Belgsir EM, Bouhier E, Yei HE, Kokoh KB, Beden B, Huser H, Leger JM (1991) Electrochim Acta 36:1157–1164
50. Dailey A, Shin J, Korzeniewski C (1998) Electrochim Acta 44:1147–1152
51. Fan YJ, Zhou ZY, Zhen CH, Fan CJ, Sun SG (2004) Electrochim Acta 49:4659–4666
52. Schnaidt J, Heinen M, Jusys Z, Behm RJ (2012) J Phys Chem C 116:2872–2883
53. Heinen M, Jusys Z, Behm RJ (2010) J Phys Chem C 114:9850–9864
54. Grgur BN, Markovic NM, Ross PN (1998) J Phys Chem B 102:2494–2501
55. Bock C, MacDougall B (2002) Electrochim Acta 47:3361–3373
56. Yang LX, Bock C, MacDougall B, Park J (2004) J Appl Electrochem 34:427–438
57. Manzo-Robledo A, Boucher AC, Pastor E, Alsono-Vante N (2002) Fuel Cells 2:109–116
58. Jayaraman S, Jaramillo TF, Baeck SH, McFarland EW (2005) J Phys Chem B 109:22958–22966
59. Maillard F, Peyrelade E, Soldo-Olivier Y, Chatenet M, Chaınet E, Faure R (2007) Electrochim Acta 52:1958–1967
60. Micoud F, Maillard F, Bonnefont A, Job N, Chatenet M (2010) Phys Chem Chem Phys 12:1182–1193
61. Chojak Halseid M, Jusys Z, Behm RJ (2010) J Electroanal Chem 644:103–109
62. Ma L, Zhaoa X, Si F, Liu C, Liao J, Liang L, Xing W (2010) Electrochim Acta 55:9105–9112
63. Wang ZB, Zuo PJ, Yin GP (2009) Fuel Cells 9:106–113
64. Wolter O, Heitbaum J (1984) Ber Bunsenges Phys Chem 88:6–10
65. Sobkowski J, Czerwinski A (1985) J Phys Chem 89:365–369
66. Leiva EPM, Santos E, Iwasita T (1986) J Electroanal Chem 215:357–367
67. Visscher W, Gootzen JFE, Cox AP, van Veen JAR (1998) Elecrochim Acta 43:533–547
68. Couto A, Rincon A, Perez MC, Guttierrez C (2001) Electrochim Acta 46:1285–1296
69. Siwek H, Lukaszewski M, Czerwinski A (2008) Phys Chem Chem Phys 10:3752–3765
70. Santiago EI, Camara GA, Ticianelli EA (2003) Electrochim Acta 48:3527–3534
71. Jiang L, Colmenares L, Jusys Z, Sun GQ, Behm RJ (2007) Electrochim Acta 53:377–389